frontiers | Frontiers in Materials

TYPE Original Research
PUBLISHED 16 September 2024
DOI 10.3389/fmats.2024.1454201

OPEN ACCESS

EDITED BY
Alireza Tabarraei,
University of North Carolina at Charlotte, United States

REVIEWED BY
Lucio Nobile,
University of Bologna, Italy
Carlos Humberto Martins,
State University of Maringá, Brazil

*CORRESPONDENCE
Mehtab Alam,
m_alam@tongji.edu.cn

RECEIVED 24 June 2024
ACCEPTED 06 September 2024
PUBLISHED 16 September 2024

CITATION
Khan M, Umar M, Alam M, Ali U, Vatin NI and Almujibah H (2024) Evaluation of design parameters for geosynthetic reinforced-soil integrated bridge system based on finite element analysis.
Front. Mater. 11:1454201.
doi: 10.3389/fmats.2024.1454201

Evaluation of design parameters for geosynthetic reinforced-soil integrated bridge system based on finite element analysis

Mahrukh Khan[1], Muhammad Umar[1,2], Mehtab Alam[3,4]*, Umair Ali[5], Nikolai Ivanovich Vatin[6] and Hamad Almujibah[7]

[1]National University of Computer and Emerging Sciences, Lahore, Pakistan, [2]Institute of Industrial Science, The University of Tokyo, Bunkyo, Japan, [3]Department of Civil Engineering, Ghulam Ishaq Khan Institute, Swabi, Pakistan, [4]Department of Geotechnical Engineering, College of Civil Engineering, Tongji University, Shanghai, China, [5]Civil and Environmental Engineering Department, King Fahd University of Petroleum and Minerals, Dhahran, Saudi Arabia, [6]Peter the Great St. Petersburg Polytechnic University, Saint Petersburg, Russia, [7]Department of Civil Engineering, College of Engineering, Taif University, Taif, Saudi Arabia

This study evaluates the performance of a geosynthetic reinforced soil integrated bridge system (GRS-IBS) in terms of total displacement by varying different design parameters simultaneously and also suggests optimum values of them. These parameters include, i. backfill internal friction angle ($Ø_b$) and reinforcement spacing (Sv), ii. Backfill internal friction angle ($Ø_b$) and geogrid axial stiffness (EA) at varying reinforcement spacing (Sv), iii. Backfill internal friction angle ($Ø_b$) and number of bearing bed layers, and the effect of retained backfill slope (m_b). Simulations were conducted using PLAXIS 2D software. Analysis showed that the cumulative effect of these parameters had a significant effect on total displacement but after a certain point increase or decrease in their values showed no effect on the results while some parameters showed negligible effect on the deformation of the wall. Furthermore, due to the notable effect of $Ø_b$, Sv and EA on the total displacement of the wall, the impact of these parameters was also investigated on the development of tensile force in the topmost layer of geogrid in GRS IBS. It was noted that the shape of the tensile force distribution graph was the same for all the cases and the order of the parameters in terms of their effect on tensile force was $S_v > Ø_b >$ EA. Also, a detailed analysis of tensile force development in all the layers of geogrids showed that if $S_v \leq 0.2$ m, the spacing between reinforcement in the lower portion of GRS IBS can be increased as these layers showed approximately zero tensile load.

KEYWORDS

geosynthetic reinforced soil integrated bridge system GRS-IBS, finite element analysis, parametric study, tensile forces, optimum parameters

1 Introduction

Due to the rise in construction, engineers have shifted their interest toward soil stabilization techniques to utilize weak soils as backfill material, for pavement and road construction or foundations (Saquib Wani and Mir, 2020; Tahasildar et al., 2018; Cao et al., 2024). There are different soil stabilization techniques including mechanical stabilization and chemical stabilization and these techniques are considered costly, Further,

chemical stabilization techniques impact the environment in many ways. For instance, lime stabilization produces a considerable quantity of carbon dioxide and calcium-based materials and the techniques that involve the use of bitumen impact the plant growth hence disturbing the agricultural activities. Therefore, at present, the use of these conventional soil stabilization techniques has limited scope because people are more concerned towards sustainable development by using cost-effective and environmentally friendly materials and techniques. Over the past few decades, the use of geosynthetics has become popular mainly due to its sustainability and cost-effectiveness. Moreover, they have also proven beneficial because of the increase in soil load-bearing capacity and resistance of soil settlements (Archibong et al., 2020; Rashid and Yousaf Shah, 2021; Du et al., 2023).

Geosynthetic Reinforced Soil (GRS) was primarily being used in slopes, retaining walls, and embankments, however, GRS is now being used as a part of an integrated bridge system and collectively is known as Geosynthetic Reinforced Soil Integrated Bridge System (GRS IBS). It is a substitute for the conventional bridge system in which load is transferred through piles to the deep strata (Abu-Hejleh et al., 2001; 2012; Mohamed et al., 2012; Saghebfar et al., 2017; Xie and Leshchinsky, 2015).

GRS IBS is built with commonly available construction materials and equipment which results in short construction time. The overall cost of GRS IBS is 60% less than conventional bridges and they also require less maintenance throughout their life span (Federal Highway Administration, 2019). Moreover, due to simpler design, these bridges can be constructed and adjusted to various environmental or unforeseen site conditions. In conventional bridges, with time, differential settlement of the approach road and bridge creates s bump at the bridge approach, whereas, this problem has been avoided in GRS IBS. In GRS IBS the slab and the roadway are meshed due to which they act as a monolithic structure and eventually the slab and road settle together (U.S. Department of transportation, 2020). The use of GRS IBS has also been promoted due to the ability to tolerate seismic loads and differential settlement in addition to cost-effectiveness and less construction period, (Adams et al., 2007; Lu et al., 2017; Kost et al., 2014; Talebi et al., 2014; Huang et al., 2022).

Talebi and Meehan, 2015 simulated several parametric model assessments to understand the behavior of GRS-IBS, using the finite element approach. The study investigated the backfill friction angles ($\emptyset_b$) (32° to 42°), cohesion (c) (5 to 25 kPa), stiffness (EA) (500 to 1,100 kN/m) and interface strength (0.3 to 1). The results of the study showed that the applied dead and live loads are the primary reason for the deformation experienced by conventional GRS-IBS structures. As reinforced soil strength increased from $\emptyset_b$ = 32° to 42°, the maximum vertical and horizontal displacement was reduced by 38% and 22%, and the maximum tension in the geotextile was reduced by 43% with a 42% increase in the safety factor. It was also noted that variations in interface rigidity had little impact on settlement. However, beyond the value of 0.6, the impact of changes in interface rigidity increased.

A parametric study using FLAC was conducted by Zheng and Fox (2017) to investigate the effects of backfill soil compaction, reinforcement length (Lr), reinforcement stiffness (EA), and bearing bed reinforcement, on the lateral facing deformations of GRS-IBS under static loading. The results of the study showed that the maximum displacement of lateral facing increases from 17.1 (for no compaction) to 21.8 mm (for heavy-weight compactor). Reinforcement length on the other hand has minimal effect on lateral-facing displacements. The maximum lateral displacement for a reinforcement length of 0.5H (where H is the Abutment height) was 18.7 mm which was slightly higher than the maximum lateral displacement against the baseline reinforcement length. After increasing the reinforcement length from 0.5H to 1.1H no change in the maximum lateral displacement was observed. Also, when reinforcement stiffness increased from 250 to 1000 kN/m, maximum lateral displacement decreased from 27 to 13 mm. Several bearing bed reinforcement layers ranging between 0 and 15 showed that maximum lateral deformation decreased from 18 mm to 16 mm. Abu-Farsakh and Ardah (2019a) investigated the performance of GRS IBS in terms of lateral facing displacement, strain distribution along reinforcement, and location of potential failure zone by 2D Finite Element (2D-FE) analysis method using PLAXIS 2D. They individually considered parameters including internal friction angle $\emptyset_b$, the width of the reinforced soil foundation, bearing bed reinforcement, and setback distance. The results showed that the internal friction angle, setback distance, and width of strip footing have a significant impact on the performance of the GRS-IBS, whereas the width of the reinforced soil foundation and the length of reinforcement have no impact on the performance of the GRS-IBS. The potential failure envelope of the GRS-IBS abutment was the combination of punching shear failure envelope (top) that starts under the inner edge of the strip footing and extends vertically downward to intersect with the Rankine active failure envelope (bottom). In a subsequent study, Abu-Farsakh et al. (2019a) performed numerical modeling of GRS IBS using PLAXIS 2D. In this research, the author individually considered the following parameters: span length, reinforcement spacings, and reinforcement stiffness. The results showed that the magnitude of maximum strain increases from 0.4% to 0.9% and maximum lateral deformation from 12 mm to 30 mm with the increase in span length from 12.2 m to 36.6 m. Similarly, the magnitude of maximum strain increases from 0.62% to 1.63%, and maximum lateral deformation from 28 mm to 42 mm with the increase in reinforcement spacing from 0.1 m to 0.4 m. In the case of reinforcement stiffness, the maximum strain decreases from 1.3% to 0.5% and lateral displacement decreases from 37 mm to 26 mm by increasing stiffness from 300 kN/m to 1500 kN/m. In another study, Abu-Farsakh et al. (2018) performed a 3D Finite Element (3d FE) analysis of GRS-IBS under different loading conditions (end of bridge construction, surface loading, abnormal loading) using PLAXIS 3D. The results of the 3D-FE model were also compared with the results of the 2D-FE model which were in good agreement. Results showed that the maximum settlement of abutment due to service load was 9 mm. The maximum lateral deformation of the wall was 3 mm and 7 mm for service load and abnormal load respectively.

Among others, Xu et al. (2020) performed a shaking table test to investigate the seismic performance of GRS IBS by considering only two parameters, i.e., reinforcement stiffness and reinforcement spacing. It was concluded that a reduction in the reinforcement spacing is more beneficial as compared to an increment in the reinforcement spacing to minimize the effect of seismic activity on GRS IBS.

In a recent study, Soo and Patinga, 2021 compared the GRS Integral Bridge (GRS-IB) that uses full height rigid (FHR) facing, GRS-IBS and a conventional integral bridge (IB) having an integral bridge system but without any reinforcement. Numerical simulations were performed using PLAXIS 2D under different loading conditions (end of construction, general traffic load, railway load). Numerical analysis showed that GRS-IB experienced the least lateral deformations of the wall as compared to the other two bridge systems. GRS IBS showed the highest lateral deformation (0.18%–0.27%) because of 0.5 m thick concrete masonry unit (CMU) blocks, whereas the other two bridge systems have 0.9 m FHR facing. This behavior of lateral deformation of bridges was similar for all the loading conditions. The main conclusion drawn from this study was the better performance of the GRS IB bridge, however, limited parameters were considered in this study.

The preceding studies have focused mainly on the performance of GRS IBS in terms of lateral facing deformations or settlements by considering parameters individually, such as friction angle, reinforcement spacing, reinforcement length, reinforcement stiffness, number of bearing bed layers, and setback distance.

A detailed investigation was needed to investigate the performance of GRS IBS in terms of total displacement (horizontal and lateral) by considering the cumulative effect of different parameters. Furthermore, it is equally important to address the optimum range of these parameters by considering their combined effect. Many studies are available for parameters such as backfill friction angle ($\emptyset_b$), reinforcement spacing (S_v), reinforcement length (L_r), reinforcement axial stiffness (EA), etc. However, few studies have been found that consider the effect of the slope of retained backfill material, on GRS-IBS performance. Hence, this research involves the evaluation of the performance of GRS IBS considering the cumulative effect of i. backfill internal friction angle $\emptyset_b$ and reinforcement spacing S_v, ii. backfill internal friction angle $\emptyset_b$ and geogrid axial stiffness EA and reinforcement spacing S_v, iii. backfill internal friction angle $\emptyset_b$ and number of bearing bed layers, and the effect of retained backfill slope m_b. Also, the behavior of tensile load has been investigated in all layers of reinforcement for a single GRS IBS bridge with S_v of 0.1 m and 0.3 m.

2 Description of the bridge model

For analysis and design of GRS-IBS, a conventional RCC approach road bridge, constructed in 2018, near Hiran Minar, district Sheikhupura, Pakistan, was selected. Figure 1 shows the complete details of the road bridge considered for this study along with the actual bridge at the site.

The GRS-IBS is designed according to the design criteria provided by the FHWA design manual (Adams and Nicks, 2018). The typical 2-dimensional GRS IBS model is shown in Figure 2. The total bridge span length was 9 m and the height of abutment was 4.2 m. Bearing width (b) was 1.2 m and the setback distance (a_b) was 0.2 m. Clear space (de) which is the gap between the top of the uppermost facing block and the bottom of the girder was selected 0.076 m. The total base width (B_{total}) used was 1.82 m which satisfies the FHWA minimum base to height (B_{total}/H) ratio criteria i.e., minimum $B_{total}/H = 0.3$. The depth of excavation for Reinforced Soil Foundation (D_{RSF}) which is calculated as $2.5B_{total}$, was 0.46 m. The facing blocks used in this study are Concrete Masonry Unit (CMU) blocks with a thickness of 0.2 m. The length of the lowest reinforcement layer at the base is 6 ft (converted into meter) and the length of the bearing bed reinforcement layer (L_{rb}) is 1.52 m. Different vertical spacings between reinforcement layers (S_v) were used for different cases to obtain optimum spacing values. The values used are 0.1, 0.2, and 0.3 m. Similarly, various geogrid axial stiffness (EA) values were used as 600 kN/m, 800 kN/m, and 1000 kN/m. Different slope values of the retained backfill (m_b) used are 1:1, 1:1.5, and 1:2. In this study, the varying number of bearing bed reinforcement layers used are 2, 4 and 6 layers. Due to the symmetrical ends of the bridge, numerical modeling of both sides of the bridge will give similar results. Therefore, in order to reduce the computational time, only one side of the bridge abutment was simulated. This method of analysis of bridge as a free-standing geometry was also conducted by Zheng and Fox (2017), Abu-Farsakh et al. (2018), Soo and Patinga, 2021, Abu-Farsakh et al. (2019b) and Huang et al. (2023). The integrated approach backfill and RC bridge girder are converted into their equivalent vertical loads. Bridge models have been simulated based on the PLAXIS 2D reference and tutorial manual (Bentley Plaxis 2d tutorial manual, 2020b; Bentley Plaxis 2d tutorial manual, 2020a).

3 Soil parameters

The bridge model comprises three types of soils, i. foundation soil, ii. reinforced backfill soil, iii. reinforced soil foundation. The model soil input parameters for foundation soil used in this study were based on the geotechnical investigation report collected from the highway department, government of Punjab. Due to the absence of data for parameters such as young's modulus and Poisson ratio for retained backfill soil and reinforced soil foundation, the values have been used based on previous studies conducted by Abu-Farsakh and Ardah (2019a); Abu-Farsakh et al. (2018); Ardah et al. (2021). Since the FEM models analyzed in these studies were validated by *in situ* results therefore in this study the range for variation of EA, $\emptyset_b$, S_v and a number of bearing bed layers have been selected based on their research.

4 Finite element modelling

Ardah et al. (2021) reported that analyzing geotechnical problems through numerical analysis has many advantages such as attaining comprehensive results, and evaluation of the effect of different parameters and loading conditions on the geotechnical problem, which is time-consuming and costly, otherwise. Therefore, the impacts of various variables on the performance of GRS-IBS to obtain their optimum values, have been examined in this study using the Finite Element Method (FEM) analysis program PLAXIS 2D Connect edition V21. Plaxis 3D offers a more comprehensive modeling platform than Plaxis 2D, especially when you have sufficient computational resources. In this study, we assumed a plane strain condition with a sufficiently large spread in the third dimension. If a similar model were developed in Plaxis 3D with

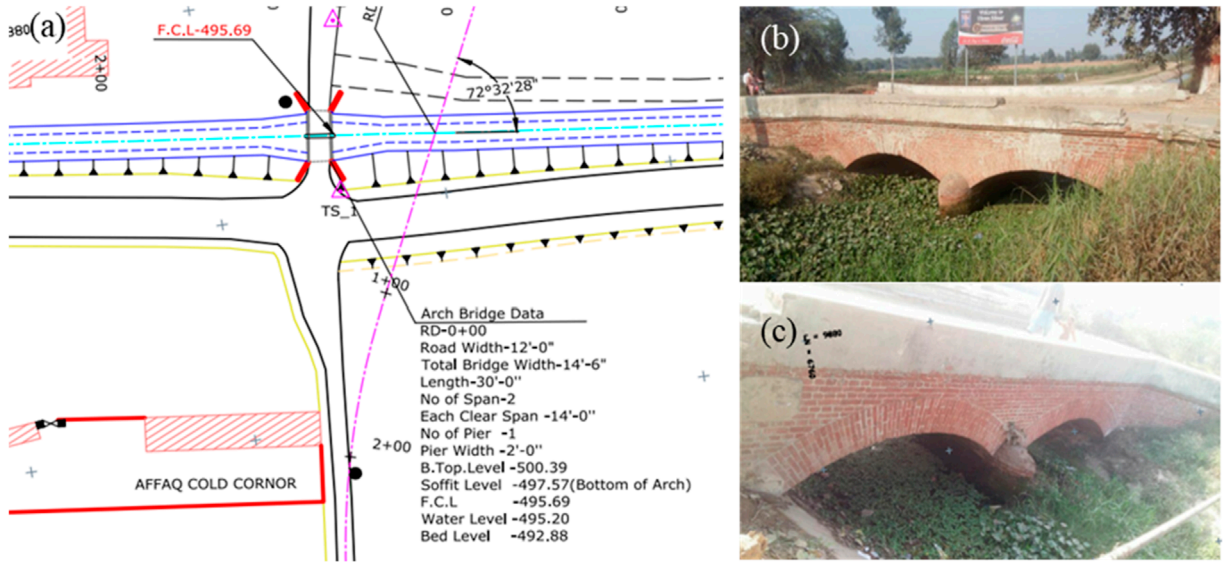

FIGURE 1
RCC approach road bridge data and actual bridge on site. **(A)** Topographic map of approach road bridge, **(B)** Upstream of bridge, **(C)** Downstream of bridge.

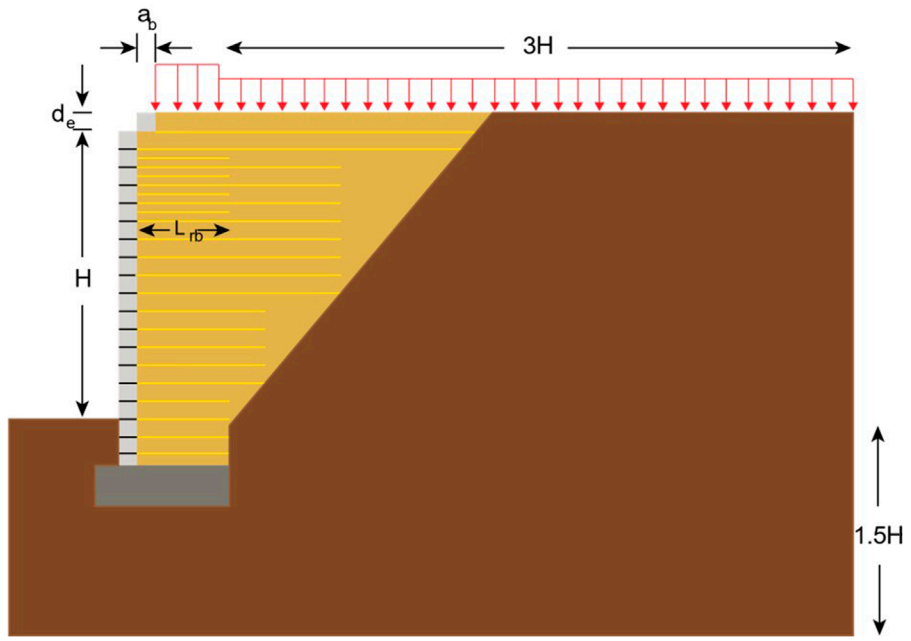

FIGURE 2
Geosynthetic Reinforced-Soil Integrated Bridge System model.

large dimensions in the third direction, the resulting deformation would likely be close to the results of the current 2D model.

There are different constitutive models for simulation of material behavior in PLAXIS including the soft soil creep model (SS), Mohr coulomb (MC), hardening soil model (HS), and linear elastic model (EM). HS model and MC model are used extensively. HS model is considered an advanced anisotropic model as this model can predict the nonlinear behavior of over-consolidated clays, loose sands, and dense sands. It is a type of hyperbolic model that results in accurate soil behavior during loading phases due to stress dependency of stiffness moduli. There are three types of soil stiffness parameters required in the HS model i.e., secant modulus (E^{ref}_{50}), oedometer modulus (E^{ref}_{oed}), and unloading reloading stiffness (E^{ref}_{ur}). HS model has been used by many of the previous researchers to simulate the backfill soil including Abu-Farsakh et al. (2018), Damians et al. (2016), and Ardah et al. (2017). MC model is a linear

TABLE 1 Model soil input parameter.

Parameters	Foundation soil	Reinforced fill soil	Reinforced soil foundation	CMU facing blocks	Geogrids
Model	Mohr Coulomb	Mohr Coulomb	Mohr Coulomb	Linear Elastic (Non porous)	—
Unit weights	19 kN/m^3	18 kN/m^3	16 kN/m^3	25 kN/m^3 (unsaturated)	—
Cohesion	24 kPa	0.1 kPa	0.0 kPa	—	—
Friction angle	28°	49°, 52°, 55°	40°	—	—
Elastic Modulus	30E3 kPa	30E3 kPa	30E3 kPa	30E6 kPa	—
Poisson Ratio	0.2	0.2	0.2	0.0	—
Axial Stiffness	—	—	—	—	600–1,000 kN/m

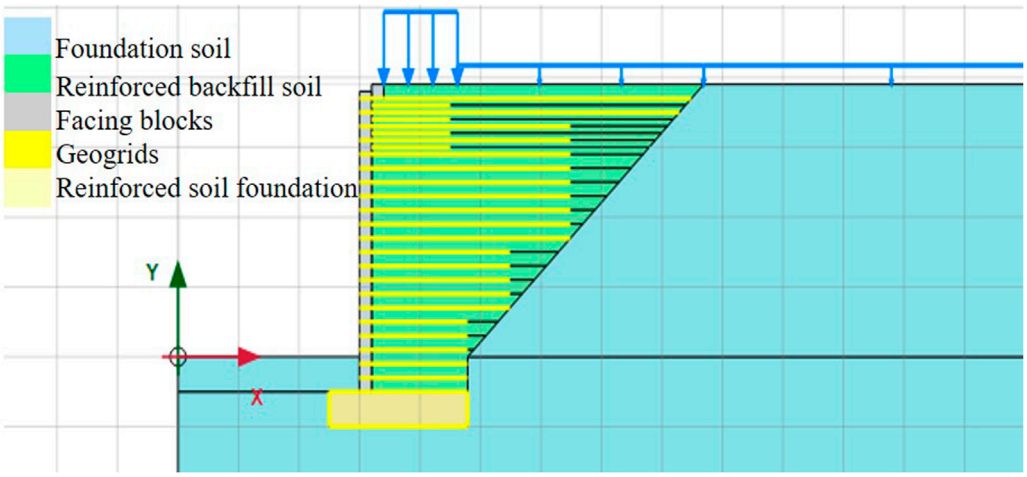

FIGURE 3
GRS IBS model on PLAXIS 2D.

elastic perfectly plastic model with the first order approximation of the soil behavior (Murtaza Rasool et al., 2023). As discussed earlier, the hardening soil model has been used for reinforced backfill soil therefore to differentiate, in this study Mohr Coulomb soil model has been selected for reinforced backfill soil. Details of the models and input parameters used are tabulated in Table 1. A layout of the GRS IBS numerical model on PLAXIS 2D has been shown in Figure 3.

4.1 Loading conditions

In this study, the numerical model has been simulated under a combination of dead and live load conditions. Dead load comprises the load of equivalent girder load along with the approach pavement. While live load comprises the load of general traffic (Traffic surcharge) calculated by employing the equation $q_t = h_{eq}\gamma_b$ (Adams and Nicks, 2018). The values used in this study are tabulated in Table 2.

TABLE 2 Load values for numerical modeling.

Loading combinations	Loading values (kPa)
Bridge DL	105
Roadway DL	18
Bridge DL + Traffic surcharge	118
Roadway DL + Traffic surcharge	31

4.2 Stagged construction

The numerical analysis of this model consists of 19 phases before the load application. In every construction phase, the deformations and built pressures were transferred to the next phase until the final phase was achieved. Before the addition of a first phase, an initial phase exists by default. The model in the initial phase has been illustrated in Figure 4A. In this phase, all the structural elements

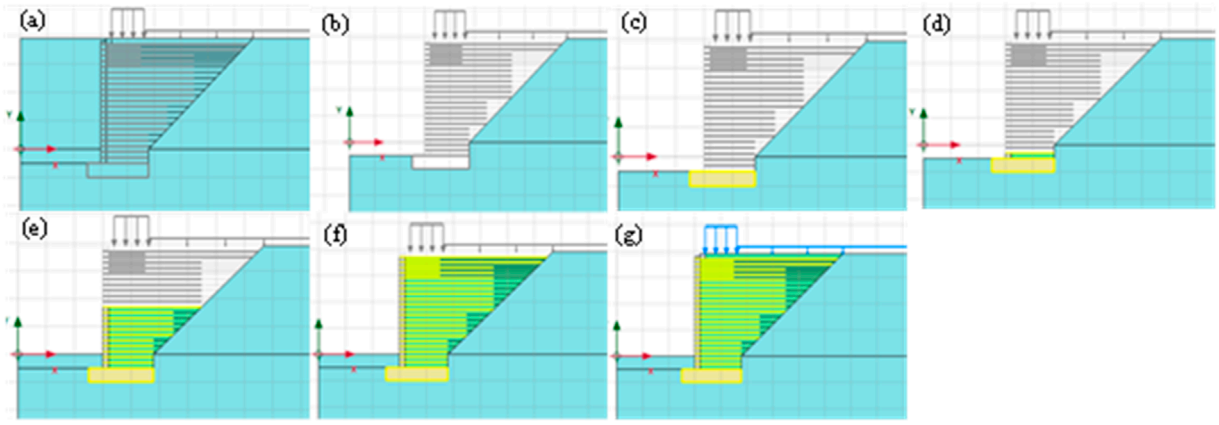

FIGURE 4
Stagged construction of GRS IBS on PLAXIS 2D. **(A)** Initial phase of model, **(B)** Phase 1 (excavation of foundation soil), **(C)** Phase 2 (construction of RSF), **(D)** Phase 3 (placement of first backfill soil layer and geogrid), **(E)** Phase 12, **(F)** Phase 19 (placement of all backfill soil layers and geogrids), **(G)** Phase 20 (activation of loads).

were deactivated and only the original foundation soil was activated. Then first phase was created which replicated the excavation of the foundation soil for bridge construction as shown in Figure 4B. Phase 2 consists of the construction of RSF as shown in Figure 4C. After this, phase 3 to phase 19 follows the same pattern, i.e., activation of facing block, activation of backfill soil, and activation of geogrid as shown in Figures 4D, E. This pattern is repeated until phase 19 is achieved as shown in Figure 4F. In phase 20, loads are also activated as shown in Figure 4G.

5 Results of numerical analysis

5.1 Effect of varying backfill angle of internal friction ($\emptyset_b$) and geogrid spacing (S_v)

Three considered values for $\emptyset_b$ were 49°, 52° and 55° and for S_v, 0.1 m, 0.2 m and 0.3 m. Figure 5 shows the simultaneous effect of both parameters on the wall deformation response of GRS IBS in terms of total displacement at 20%, 40%, 60%, and 80% of the abutment height.

It can be seen that for S_v = 0.1 m, the maximum displacement at 0.8H increased from 22 to 26 mm for $\emptyset_b$ ranging from 55° to 49°. Similarly, at the same height and $\emptyset_b$ values the maximum displacement increased from 27 to 32 mm (20% to 23%) by increasing S_v from 0.1 to 0.2 m. Abu-Farsakh et al. (2019b) also showed an increase in total displacement throughout the wall height by increasing S_v. Furthermore, for the same $\emptyset_b$ values (i.e., 55°, 52°, 49°) the maximum displacement increased by approximately 40% to 45% when S_v increased from 0.1 m to 0.3 m. When S_v = 0.3 m there was an insignificant effect on displacement throughout the wall height for $\emptyset_b$ = 52° and 55°. This shows that the wall displacement depends on the backfill angle of internal friction and spacing of the geogrid. Furthermore, after a certain geogrid spacing, increasing the backfill angle of internal friction does not contribute to the wall displacement.

5.2 Effect of varying backfill angle of internal friction ($\emptyset_b$) and geogrid stiffness (EA)

The effect of varying $\emptyset_b$ and EA was observed at three S_v values of 0.1 m, 0.2 m, and 0.3 m. Three considered values for $\emptyset_b$ were 49°, 52° and 55° and for EA, 600 kN/m, 800 kN/m, and 1000 kN/m. Figure 6 shows the simultaneous effect of both parameters on the wall deformation response of GRS IBS in terms of total displacement at 20%, 40%, 60%, and 80% of the abutment height when S_v = 0.1 m.

The figure showed that when $\emptyset_b$ = 49°, maximum displacement at 0.8H varied from 22 to 26 mm for EA varying from 1000 kN/m to 600 kN/m. A study conducted by Abu-Farsakh and Ardah (2019a) also showed an increase in total displacement throughout the wall height by decreasing EA. At the same height, the displacement decreased 20 to 24 mm (i.e., 5% to 10%) for the same EA values when $\emptyset_b$ increased from 49° to 52°. For all EA values, an additional reduction of 10% to 15% in total displacement was observed when $\emptyset_b$ was increased from 52° to 55°. It is important to note that at $\emptyset_b$ = 49°, an insignificant effect of 4% on maximum displacement was observed with the increase of EA from 800 kN/m to 1,000 kN/m. Also, at $\emptyset_b$ = 52° and 55°, there was no change in total displacement values at 20%, 40%, 60%, and 80% of the abutment height at EA = 1,000 kN/m. The graphical representation in Figure 7 shows the effect of varying $\emptyset_b$ and EA with S_v = 0.2 m on total displacement at 20%, 40%, 60%, and 80% of the abutment height.

The maximum displacement at 0.8H when $\emptyset_b$ = 49° varied from 25 mm to 32 mm for EA ranging from 1000 kN/m to 600 kN/m. At the same height, the maximum displacement was reduced by only 4% for 1000 kN/m but remained constant for 600 kN/m and 800 kN/m when $\emptyset_b$ increased from 49° to 52°. When $\emptyset_b$ increased from 52° to 55° the maximum displacement dropped to 22 mm. The above two cases show that after specific geogrid stiffness, increasing the backfill angle of internal friction does not contribute to the wall displacement which can be due to less S_v.

The graphical representation in Figure 8 shows that the effect of varying $\emptyset_b$ and EA with S_v = 0.3 m on total displacement at

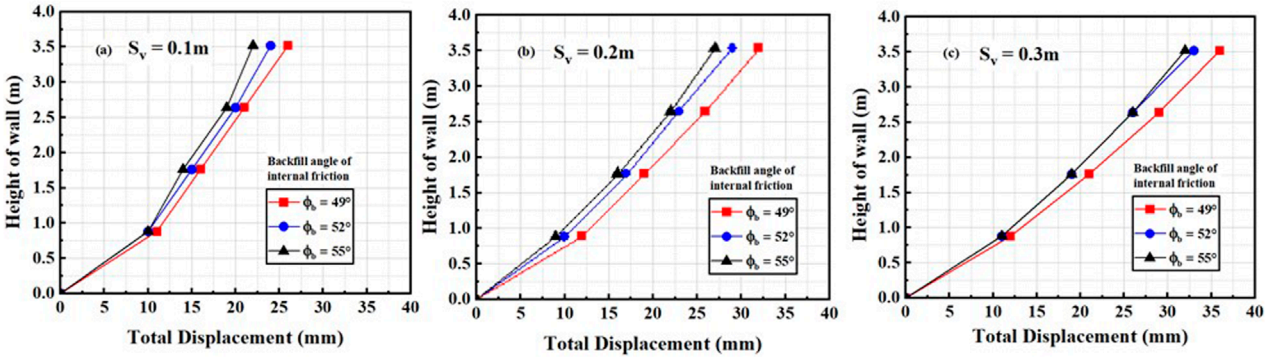

FIGURE 5
Relationship between total displacement and height of the wall by varying vertical spacing between geogrids for **(A)** S_v = 0.1m, **(B)** S_v = 0.2m, and **(C)** S_v = 0.3m.

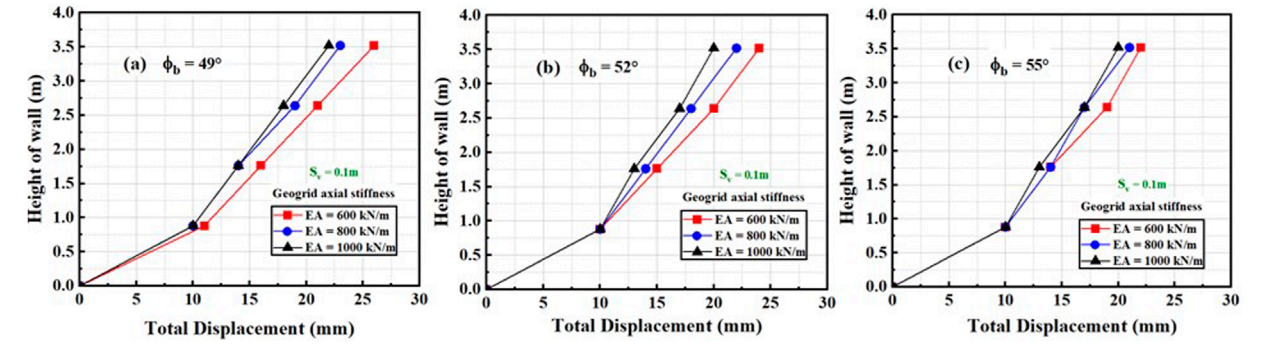

FIGURE 6
Relationship between total displacement and height of the wall by varying geogrid axial stiffness (S_v = 0.1 m) for **(A)** $\emptyset_b$ = 49, **(B)** $\emptyset_b$ = 41, and **(C)** $\emptyset_b$ = 55.

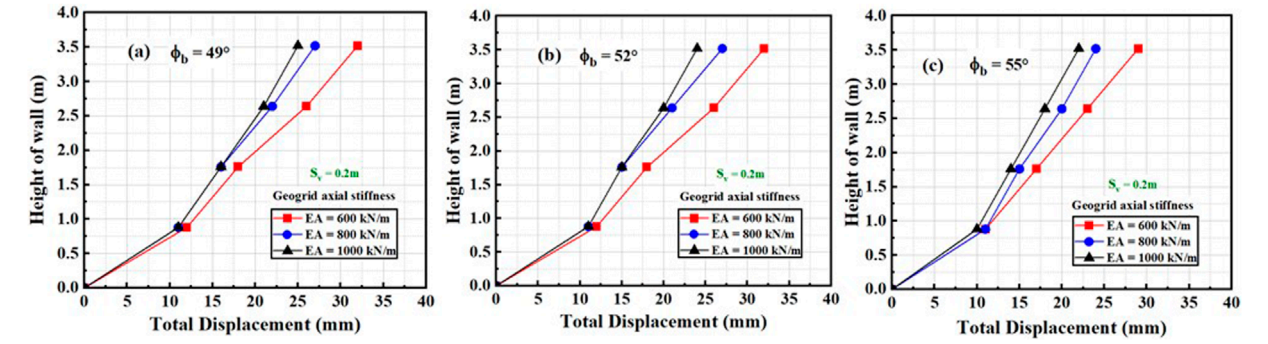

FIGURE 7
Relationship between total displacement and height of the wall by varying geogrid axial stiffness (S_v = 0.2 m) **(A)** $\emptyset_b$ = 49, **(B)** $\emptyset_b$ = 41, and **(C)** $\emptyset_b$ = 55.

20%, 40%, 60%, and 80% of the abutment height. The maximum displacement at 0.8H at $\emptyset_b$ = 49° varied from 29 mm to 37 mm for EA ranging from 1000 kN/m to 600 kN/m. The maximum displacement was reduced by 10% to 15% for all the EA values i.e., 26 mm to 33 mm when $\emptyset_b$ was increased from 49° to 52°. Similarly, an additional drop of 15% to 20% in maximum displacement values was

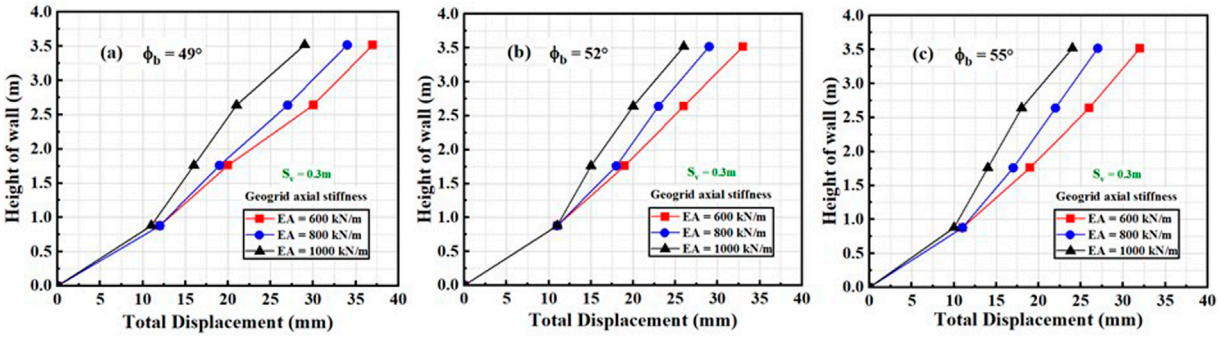

FIGURE 8
Relationship between total displacement and height of the wall by varying geogrid axial stiffness (S_v = 0.3 m) for **(A)** $\emptyset_b$ = 49, **(B)** $\emptyset_b$ = 41, and **(C)** $\emptyset_b$ = 55.

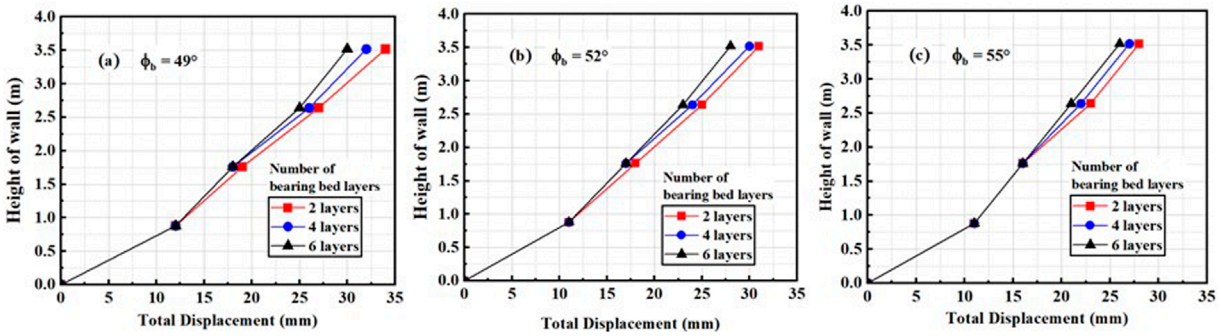

FIGURE 9
Relationship between total displacement and height of the wall by varying number of bearing bed layers for **(A)** $\emptyset_b$ = 49, **(B)** $\emptyset_b$ = 41, and **(C)** $\emptyset_b$ = 55.

observed when $\emptyset_b$ was increased from 52° to 55°. This shows that the wall displacement depends on the backfill angle of internal friction and geogrid stiffness.

5.3 Effect of varying backfill angle of internal friction ($\emptyset_b$) and no. of bearing bed layers

The bearing bed reinforcement zone is located underneath the bridge seat in GRS IBS. These bearing bed layers act as embedded footing in the reinforced soil and support large bridge loads (Adams and Nicks, 2018). Previous analysis carried out by Abu-Farsakh and Ardah (2019a) was limited to the analysis showing the (which) effects with and without bearing bed layers. However, in this study, three different bearing bed layers were analyzed, i.e., 2, 4, and 6. Similarly, $\emptyset_b$ was considered as 49°, 52° and 55°. The total displacement at 20%, 40%, 60%, and 80% of the abutment height considering the varying values of both parameters is shown in Figure 9.

Results showed that for $\emptyset_b$ = 49°, the value of maximum displacement at 0.8H is 34 mm for 2 bearing bed layers. A reduction of 6% in the value was observed when no. of bearing bed layers was doubled. Furthermore, an additional drop of 6% was observed i.e., to 30 mm when the no. of bearing bed layer increased from 4 to 6. Increment in $\emptyset_b$ from 49° to 52° showed a drop of 6% to 12% in the value of maximum displacement at 0.8H. It varied between 31 mm and 28 mm for 2 to 6 layers respectively. At $\emptyset_b$ = 52°, an insignificant effect of 3% on the displacement was observed by increasing the number of bearing bed layers from 2 to 4. Similarly, at $\emptyset_b$ = 55°, the value of maximum displacement at 0.8H further reduced by almost 13% to 20%, i.e., 26 mm for 6 layers while for 2 layers, its value is 28 mm. However, at $\emptyset_b$ = 55°, an insignificant effect of 2 mm was observed on the displacement by increasing or decreasing the number of bearing bed reinforcement layers. Abu-Farsakh and Ardah (2019a) studied the effect on GRS IBS performance by removing and including bearing bed layers. Overall results showed that the inclusion of bearing bed layers improved the performance of GRS IBS but at higher values of $\emptyset_b$ increasing bearing bed layers from 2 to 4 showed negligible effect on total wall displacement.

5.4 Effect of varying retained backfill slope (m_b)

Backfill and reinforcement create a substructure to bear the load from the superstructure (National concrete masonary association, 2019). Figure 10 shows the effect of different m_b on maximum displacement at 20, 40, 60% and 80% of the abutment height It was

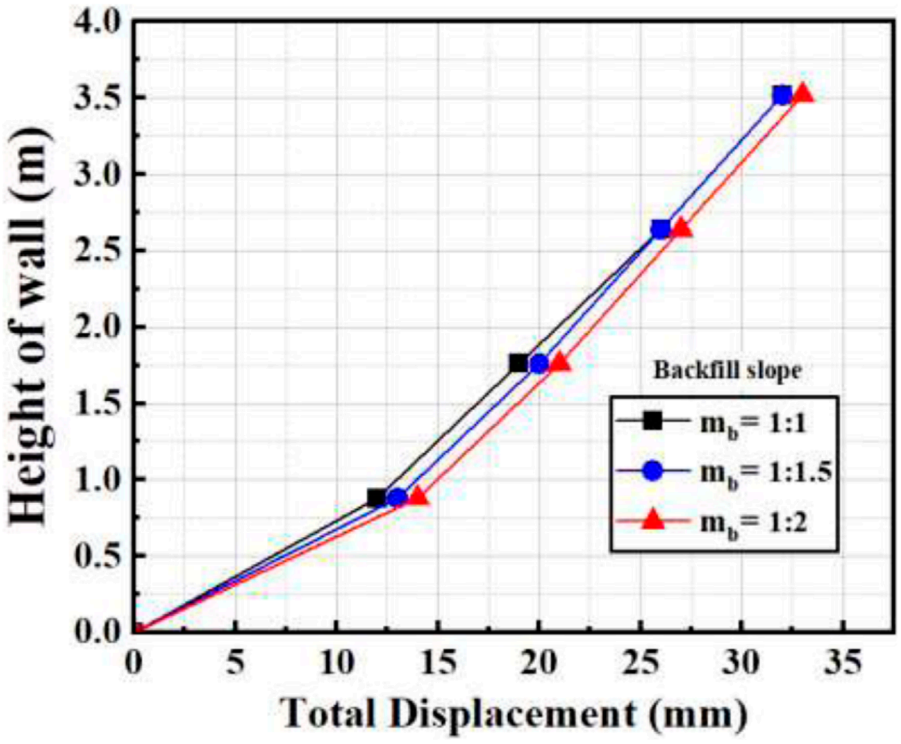

FIGURE 10
Relationship between total displacement and height of wall by varying backfill slope.

observed that the magnitude of the displacement decreases only 3% at all heights of the wall as the slope gets steeper. Furthermore, no effect on the total displacement was observed at the retained backfill slope of 1:1 and 1:1.5.

6 Discussion of results

6.1 Comparison of FEM and physical model tests

The results from the finite element model must be validated to ensure that the proposed geometry, elements, and mesh refinement are adequate for accurate analysis. Typically, this validation involves comparing the model's results with field or laboratory test data. However, due to the unavailability of such data, the results of the present study were validated by comparison with the findings of Abu Farsakh et al. (2019), who conducted a parametric study incorporating both field experiments and numerical analysis to examine the effects of reinforcement spacing and stiffness on bridge displacement.

Table 3 shows the comparison between the results of this study with the findings of Abu Farsakh et al. (2019). It can be observed from Table 3 that there is good agreement between the two studies. For instance, for a reinforcement spacing of 0.3 m, the displacement in this study is 35 mm, while 33 mm was observed by Abu Farsakh et al. (2019). Similarly, for a geogrid axial stiffness of 600 kN/m, both studies produced comparable displacement values—32 mm in this study and 32.5 mm in the study by Abu Farsakh et al. (2019). The slight difference between the results may be attributed to the use of a backfill friction angle ($Ø_b$) of 51° in the study by Abu Farsakh et al. (2019), while our study used a backfill friction angle of 52°. Additionally, differences in bridge dimensions between the two studies could also contribute to the observed variations in results.

6.2 Soil-geogrid intereation

Tensile forces from the soil are transferred to the geogrids through the mechanism of interaction. Geogrid takes these forces dominantly in one direction (if it is uniaxial geogrid) or both directions (if it is biaxial geogrid) (Mulabdic et al., 2018). The above cumulative parametric study of the following parameters (i.e., $Ø_b$, S_v, and EA) showed that these parameters have a profound influence on the total displacement of GRS IBS. Therefore, these parameters were further analyzed to study their effect on tensile forces developed in geogrids. A simplified analysis for the tensile load distribution in the topmost geogrid reinforcement layer was done. For this, three different cases were considered. In case 1, the effect was studied by considering varying $Ø_b$ (49°, 52° and 55°). In case 2, varying S_v (0.1 m, 0.2 m and 0.3 m) and in case 3, different EA (600 kN/m, 800 kN/m and 1,000 kN/m) were considered.

The tensile load distribution along the length of reinforcement measured from the back of the facing block by varying spacing of reinforcement layers is shown is Figure 11.

TABLE 3 Comparison between experimental and theoretical results.

Parameter	Experimental results (Abu Farsakh et al. (2019a))	This study
Spacing (m)	Displacement (mm)	
0.1	28	24
0.2	32	29
0.3	35	33
Geogrid axial stiffness (kN/m)		
600	32	32.5
800	27	27.5
1000	30	24

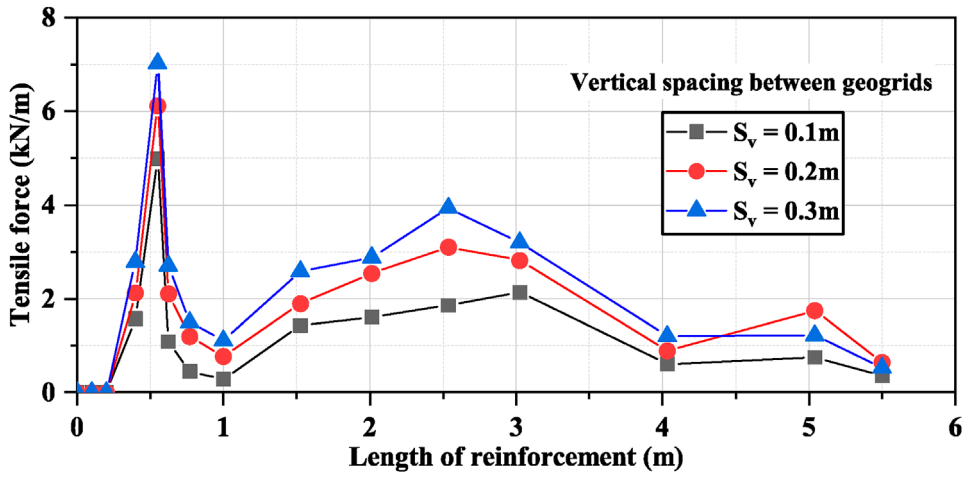

FIGURE 11
Effect of varying geogrid spacings on the tensile load of the topmost reinforcement layer.

It was observed that the trend of the graph is similar for all the considered spacings with the maximum tensile load at 0.55 m of the reinforcement length. When the spacing increased from 0.1 m to 0.2 m, the maximum tensile load increased by 23%, and when it increased from 0.2 m to 0.3 m the tensile load increased by 15%. With narrow reinforcement spacing, the number of layers of geogrids increases which causes an additional confining stress to the soil therefore, stress distribution on each soil layer will also increase. Hence due to friction action and interlocking between soil particles and geogrid layers in case of narrow spacing, the geogrids distribute the tensile load to the surrounding soil (Dulal and Kumar Yadav, 2021). This results in the composite behavior of GRS IBS and therefore, the internal stability of GRS abutments increases at close-spaced layers (Wu and Pham, 2013; Zheng et al., 2018). Abdullah et al. (2023) found that as the geogrid spacing decreases, the tensile forces in geogrids also decrease. A similar relationship was observed between geogrid tensile forces and spacing from the above analysis.

The effect of $Ø_b$ on the tensile load distribution along the length of reinforcement is shown in Figure 12.

The simulations were conducted at $Ø_b$ = 49°, 52° and 55°. It was observed that the maximum tensile load for all the considered $Ø_b$ values were at 0.55 m of the reinforcement length. When the $Ø_b$ increased from 49° to 52°, the maximum tensile load decreased by 13% and when it was increased from 52° to 55° the tensile load further decreased by 8.8%. The results indicated that maximum tensile forces in geogrids decrease with increasing $Ø_b$. This is because the greater value of $Ø_b$ means higher shear strength of backfill soil which allows it to carry a greater fraction of the applied load (Abdullah et al., 2023; Zheng et al., 2018). The relationship observed between geogrid tensile forces and $Ø_b$ from the above analysis endorse the results of study conducted by Zheng et al. (2018).

Figure 13 shows the tensile load distribution along the length of reinforcement by varying EA. A negligible effect was observed by varying EA on the tensile load of the reinforcement layer.

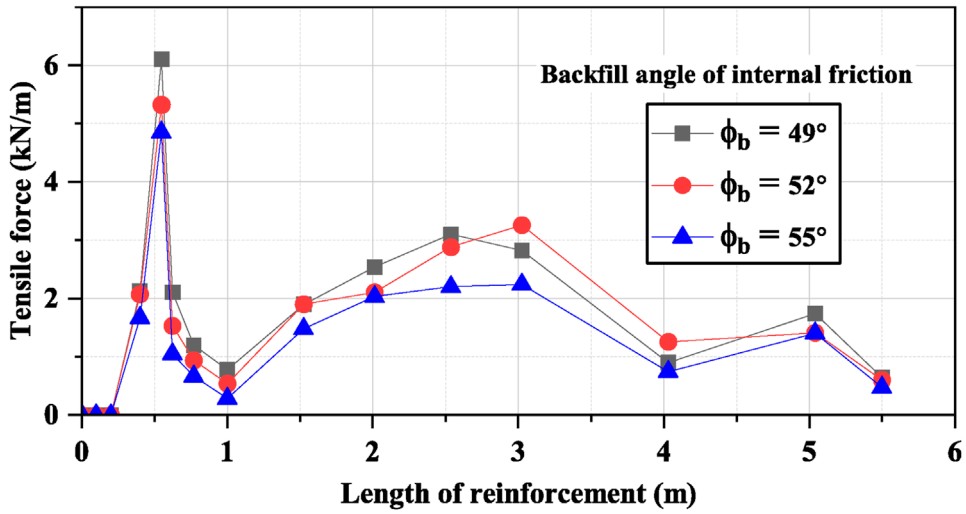

FIGURE 12
Effect of varying angle of internal friction on tensile load of topmost reinforcement layer.

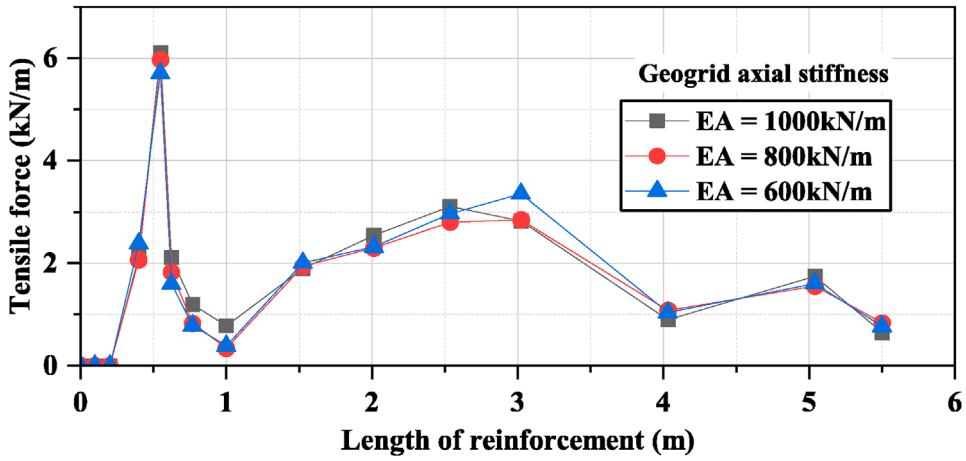

FIGURE 13
Effect of varying geogrid axial stiffness on the tensile load of the topmost reinforcement layer.

The maximum tensile load occurred at the length of 0.55 m of the reinforcement length. It was noted that when the EA increased from 600 kN/m to 800 kN/m, the maximum tensile load increased by only 5%, and when it was increased from 800 kN/m to 1000 kN/m the maximum tensile load further increased by only 2%. The results indicated that there is a direct relationship between maximum tensile forces in geogrids and EA. The relationship observed between geogrid tensile forces and EA from the above analysis following the study conducted by Zheng et al. (2018).

The above analysis showed that the maximum tensile load values occurred immediately behind the modular facing block (i.e., at a distance of 0.55 m) which can be attributed to the connection loads and application of D.L and L.L. Moreover, changes in S_v had a greater effect on geogrid tensile forces. However, increasing EA had a negligible effect on the tensile forces. Abu-Farsakh et al. (2019b) found that reinforcement spacing of 0.2 m or less, controls the performance of GRS-IBS as compared to geogrid axial stiffness. He further suggested that 0.2 m is a threshold value responsible for the composite behavior of GRS IBS which can also be verified from this study.

Since, the change of S_v had a greater effect on geogrid tensile forces, a detailed analysis was done to observe the effect of varying S_v on tensile load distribution of all the geogrid layers. Hence, two GRS IBS with S_v = 0.1 m and 0.3 m were selected. The rest of the parameters of the bridge were the same i.e., $\emptyset_b$ = 49° and EA = 600 kN/m. Furthermore, the tensile load graph was bifurcated according to the identical effect of tensile load in all the layers of geogrids. GRS IBS with S_v 0.1 m has 38 layers of geogrids. Figure 14A shows that starting from the bottom, layer no. 1 to layer no. 5 had similar behavior with tensile load values of approximately 0 throughout the geogrid length. This is possible due to the compact behavior of GRS with less S_v. Hence a greater portion

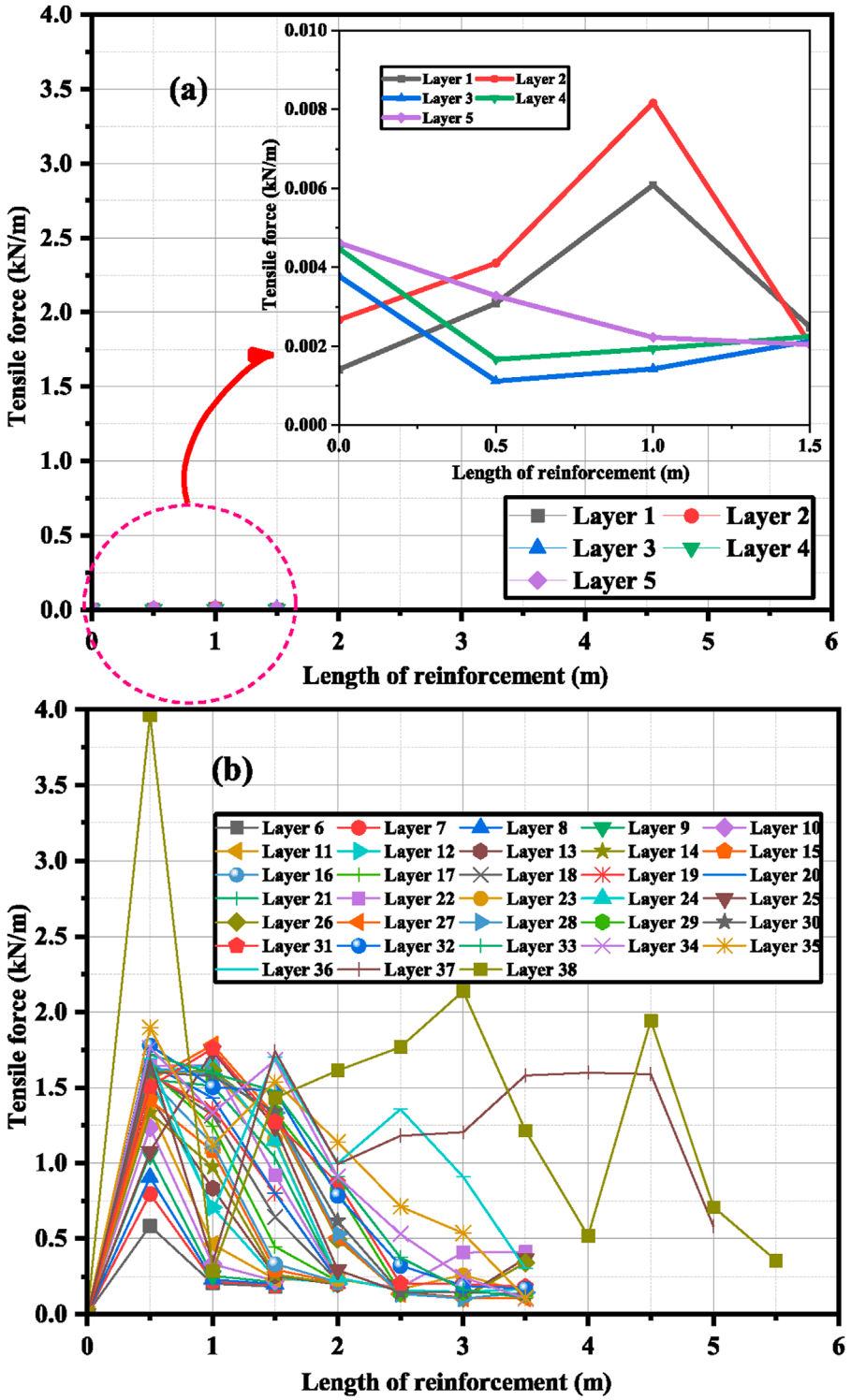

FIGURE 14
Tensile load distribution along the length of geogrids with spacing = 0.1 m. **(A)** Tensile load for layer 1 to layer 5, **(B)** Tensile load for layer 6 to layer 38.

of the load was distributed among mid portion of the wall. This can be verified by the trend of the tensile load graph obtained for layer no. 6 to layer no. 38.

Figure 14B shows that the maximum tensile load values occurred at a reinforcement length of 0.5 m. The major portion of tensile load was distributed from geogrid length of 0.5 m to 1.5 m after which a significant reduction in the load was observed except for layer no. 37 and layer no. 38, since these layers were provided immediately below the slab, hence the load was distributed from a geogrid length of 0.5 m to 3 m. The above discussion shows that if

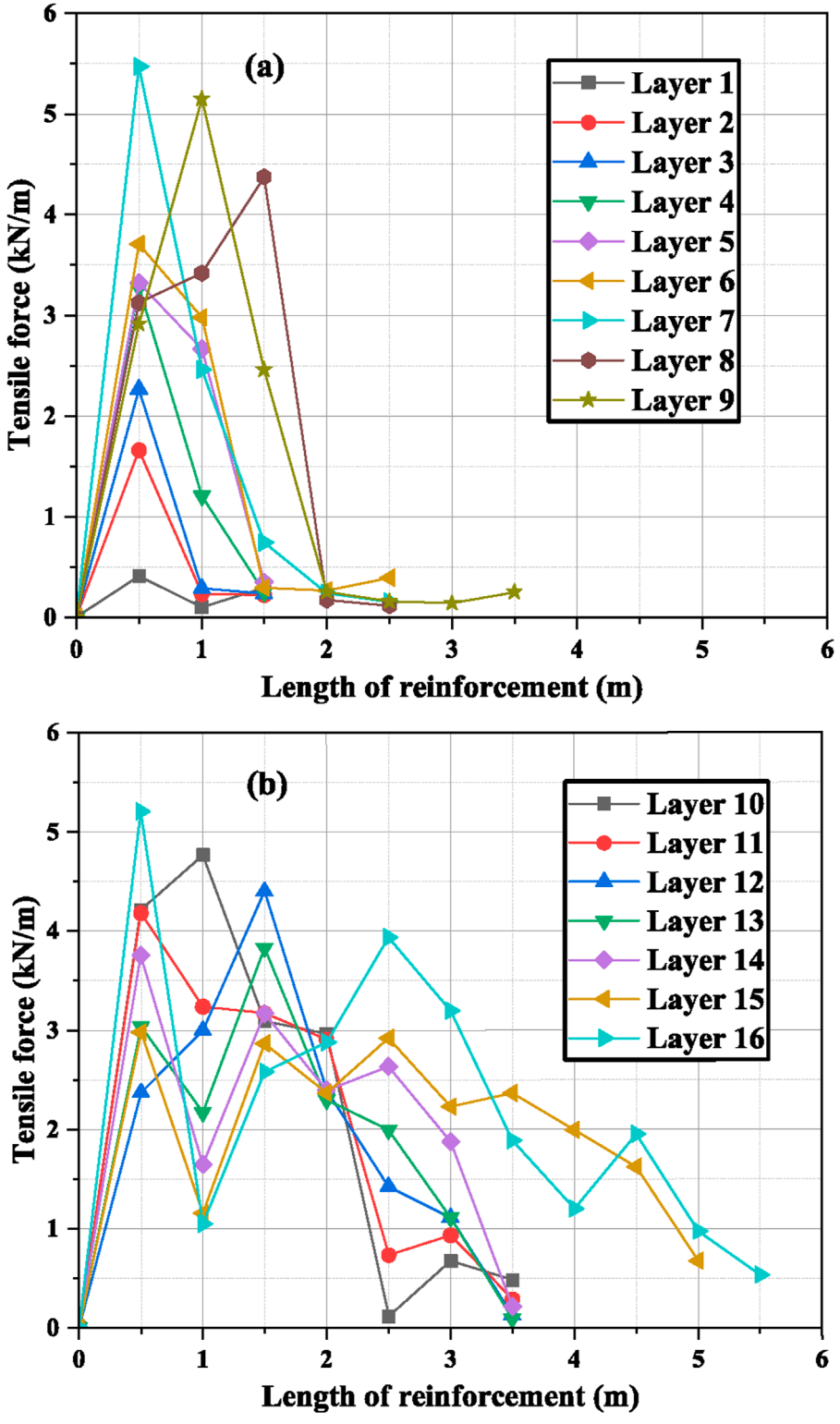

FIGURE 15
Tensile load distribution along the length of all the layers of geogrids with spacing = 0.3 m. **(A)** Tensile load for layer 1 to layer 9, **(B)** Tensile load for layer 10 to layer 16.

S_v is 0.1 m, the length of geogrids in the lower portion of the wall with approximately 0 tensile loads can be decreased or to make the structure economical, S_v in lower portion can be increased up to layer no. 5.

Similarly, GRS IBS with reinforcement spacing of 0.3 m has 16 layers of geogrids. Figure 15A shows that layer no. 1 to layer no. 9 had a similar trend with peak tensile load values at a reinforcement length of 0.5 m. The major portion of the tensile load was distributed

TABLE 4 Optimum parameters for the settlement range of 20 to 25 mm.

20 mm to 25 mm			
Phi (degrees)	49	52	55
Spacing (m)	0.1–0.2	0.1–0.2	0.2–0.3
Axial Stiffness (kN/m)	800–1,000	800–1,000	600–1,000
Slope	1:1	1:1	1:1
No. of bearing bed layers	6	6	6

TABLE 5 Optimum parameters for the settlement range of 26 to 30 mm.

26 mm to 30 mm			
Phi (degrees)	49	52	55
Spacing (m)	0.1–0.2	0.1–0.3	0.1–0.3
Axial Stiffness (kN/m)	600–800	600–1,000	600–800
Slope	1:1	1:1	1:1
No. of bearing bed layers	6	4–6	2–6

TABLE 6 Optimum parameters for the settlement range of 31 to 40 mm.

31 mm to 40 mm			
Phi (degrees)	49	52	55
Spacing (m)	0.2–0.3	0.2–0.3	0.3
Axial Stiffness (kN/m)	600–800	600	600
Slope	1:1	1:1	1:1
No. of bearing bed layers	2	2	0

from a geogrid length of 0.5 m to 1.5 m after which a significant reduction in the load was observed. This indicates that the lengths of layer no. 6 to layer no. 9 can be decreased. The trend of the load distribution was almost identical in the remaining layers starting from 10 to layer no.16. A rise and fall in tensile load values can be observed in Figure 15B which is possible due to the presence of 6 layers of bearing bed from layer 11 to layer 16.

6.3 Proposed GRS-IBS design parameters

The results obtained from parametric analysis, the optimum values of $Ø_b$, S_v, EA, number of bearing bed layers, and m_b are selected for three settlement ranges, i.e., 20 to 25 mm, 26 to 30 mm, and 31 to 40 mm. These settlement ranges have been selected based on the usage of bridges in cities and remote areas. Areas where negligible tolerance in settlement of the bridge is needed fall under the range of 20 to 25 mm. Such areas where a small amount of settlement can be allowed depending upon the usage of a bridge, fall under the range of 26 to 30 mm. In such areas where there is no heavy traffic flow, especially in remote areas (rural), the bridges can be built with a settlement ranging between 31 and 40 mm. The values for the optimum parameters are tabulated in Tables 4–6.

It can be observed that for each settlement range, the value of $Ø_b$ can be selected from 49° to 55°. Each value of $Ø_b$ is further dependent upon S_v, EA, slope, and number of bearing bed layers. Table 4 shows the optimum parameters for the settlement range of 20 mm to 25 mm. The values of the optimum parameters for $Ø_b$ 49° and 55° are equal since the analysis for both cases showed approximately similar results. Furthermore, in the case of $Ø_b$ 55°, S_v can be used from 0.1 to 0.3 m with a good margin of EA of 600 to 1,000 kN/m. It can be noticed that the value of the number of bearing bed layers remained the same for all three values of $Ø_b$. Table 5 shows the optimum parameters for the settlement range of 26 mm to 30 mm. The values of the optimum parameters for $Ø_b$ = 49° and 55° are approximately similar. The difference can be found in $Ø_b$ = 52° were S_v of 0.3 m can be used with EA of 1000 kN/m. Also, 4 number of bearing beds can be used if $Ø_b$ = 52° is to be used. Furthermore, in the case of $Ø_b$ = 55°, S_v can be used from 0.2 m to 0.3 m with EA = 600 kN/m to 800 kN/m. It can be noticed that the value of the number of bearing bed layers further dropped to 2 in the case of $Ø_b$ = 55°.

Table 6 shows the optimum parameters for the settlement range of 31 mm to 40 mm. The values of the optimum spacing for $Ø_b$ as 49° and 55° are similar but the difference can be found in $Ø_b$ = 52° where at S_v = 0.2 m, EA of 600 kN/m can be used. Also, 2 number of bearing beds can be used for this settlement range due to the higher tolerance range of settlement. Furthermore, in the case of $Ø_b$ = 55°, 0.3 m S_v can be used with an EA of 600 kN/m. It can be noticed that for this case, the provision of a bearing bed layer will not increase the overall settlement of the structure.

7 Conclusion

In this study, the effect of variation of different parameters on the performance of GRS IBS was analyzed, in terms of total displacement, and their effect on tensile load distribution in geogrid reinforcement layers was studied. Based on the parametric study, the optimum values of each parameter were selected. The main conclusions drawn from the series of analyses are as follows:

1. Although with the increase in $Ø_b$ total displacement throughout the wall decreases but varying $Ø_b$ along with S_v show that if S_v = 0.3 m varying $Ø_b$ from 52 to 55 has a negligible effect on the total displacement.
2. Adjustments in m_b can be made as per site conditions as varying m_b has an insignificant effect on the total displacement of the wall.
3. If S_v is <0.2 m, the spacing between reinforcement in the lower portion of GRS IBS (immediately above RSF) can be decreased as these reinforcement layers showed 0 tensile loads.
4. Change in S_v has a significant effect on geogrid tensile forces as compared to $Ø_b$ and EA. However, increasing EA shows a negligible effect on the tensile forces of geogrids.

In terms of displacement, out of all the parameters, 3 had a significant effect. 1. Backfill friction angle, 2. Spacing between geogrids, and 3. Axial stiffness of geogrids.

Future research work could additionally examine the impact of these parameters by considering the following recommendations:

1. The performance of GRS IBS can be further analyzed by considering varying dynamic loads and reinforcement spacings simultaneously.
2. The performance of laboratory tests can be done to obtain the required input parameters for the software to do a more realistic analysis of the performance of GRS IBS.
3. These results can be further verified by applying optimization techniques considering cost and performance, and later a software tool can be developed to quickly obtain optimum parameter values for GRS IBS by using required settlement values.

Data availability statement

The raw data supporting the conclusions of this article will be made available by the authors, without undue reservation.

Author contributions

MK: Conceptualization, Formal Analysis, Investigation, Methodology, Supervision, Writing–original draft, Writing–review and editing. MU: Data curation, Investigation, Methodology, Supervision, Writing–review and editing. MA: Formal Analysis, Investigation, Methodology, Resources, Supervision, Validation, Writing–review and editing. UA: Data curation, Validation, Writing–review and editing. NV: Funding acquisition, Resources, Writing–review and editing. HA: Resources, Writing–review and editing.

Funding

The author(s) declare that financial support was received for the research, authorship, and/or publication of this article. The research is partially funded by the Ministry of Science and Higher Education of the Russian Federation as part of the World-class Research Center program Advanced Digital Technologies (contract No. 075-15-2022-311 dated 20.04.2022). Also, this research was partially funded by Taif University, Saudi Arabia, Project No. (TU-DSPP-2024-33).

Acknowledgments

The authors extend their appreciation to Taif University, Saudi Arabia, for supporting this work through project number (TU-DSPP-2024-33).

Conflict of interest

The authors declare that the research was conducted in the absence of any commercial or financial relationships that could be construed as a potential conflict of interest.

Publisher's note

References

Abdullah, N., Ng, K., Jais, I., and Idrus, J. (2023). Use of geosynthetic reinforced soil-integrated bridge system to alleviate settlement problems at bridge approach: a review. *Phys. Chem. Earth* 129, 103304. doi:10.1016/j.pce.2022.103304

Abu-Farsakh, M., and Ardah, A. (2019a). "Finite element parametric study on the performance of geosynthetic reinforced soil–integrated bridge system (GRS-IBS)," in Geosynthetics conference. Houston, 2019 (IEEE).

Abu-Farsakh, M., Ardah, A., and Voyiadjis, G. (2018). 3D finite element analysis of the geosynthetic reinforced soil-integrated bridge system (GRS-IBS) under different loading conditions. *Transp. Geotech.* 15, 70–83. doi:10.1016/j.trgeo.2018.04.002

Abu-Farsakh, M., Ardah, A., and Voyiadjis, G. (2019a). Evaluating the performance of geosynthetic reinforced soil-integrated bridge system (GRS-IBS) under working stress condition. *MATEC Web Conf.* 271, 02001. doi:10.1051/matecconf/201927102001

Abu-Farsakh, M., Ardah, A., and Voyiadjis, G. (2019b). Numerical parametric study to evaluate the performance of a geosynthetic reinforced soil–integrated bridge system (GRS-IBS) under service loading. *Transp. Geotech.* 20, 100238. doi:10.1016/j.trgeo.2019.04.001

Abu-Hejleh, N., Outcalt, W., Wang, T., and Zornberg, G. (2001). *Performance of geosynthetic reinforced walls supporting the founders/meadows bridge and approaching roadway structures- report 1: design, materials, construction, instrumentation, and preliminary results*. Colorado, USA: Publication CDOT-DTD-R-2001-12, Colorado Department of Transportation.

Abu-Hejleh, N., Wang, T., and Zornberg, J. (2012). Performance of geosynthetic-reinforced walls supporting bridge and approaching roadway structures. *Geo Denver*, 218–243. doi:10.1061/40515(291)15

Adams, M., and Nicks, J. (2018). *Design and construction guidelines for geosynthetic reinforced soil abutments and integrated bridge systems*. U.S. Department of transportation, Federal highway administration. Available at: https://www.fhwa.dot.gov/publications/research/infrastructure/structures/bridge/17080/17080.pdf.

Adams, M., Schlatter, W., and Stabile, T. (2007). *Geosynthetic reinforced soil integrated abutments at the bowman road bridge in defiance county*. Ohio: Geo-Denver, 1–10. doi:10.1061/40909(228)12

Archibong, G., Uzoamaka Sunday, E., Akudike, J., and Okeke, O. (2020). A review of the principles and methods of soil stabilization. *Int. J. Adv. Acad. Res.* 6, 89–115.

Ardah, A., Abu-Farsakh, M., and Voyiadjis, G. (2017). Numerical evaluation of the performance of a geosynthetic reinforced soil-integrated bridge system (GRS-IBS) under different loading conditions. *Geotext. Geomembr.* 45, 558–569. doi:10.1016/j.geotexmem.2017.07.005

Ardah, A., Abu-Farsakh, M., and Voyiadjis, G. (2021). Numerical parametric study of geosynthetic reinforced soil integrated bridge system (GRS IBS). *Geotext. Geomembr. 49289-03* 49, 289–303. doi:10.1016/j.geotexmem.2020.10.005

Bentley Plaxis 2d reference manual (2020a). Available at: https://communities.bentley.com/cfs-file/__key/communityserver-wikis-components-files/00-00-00-05-58/3113.PLAXIS2DCE_2D00_V20.02_2D00_2_2D00_Reference.pdf

Bentley Plaxis 2d tutorial manual (2020b). Available at: https://communities.bentley.com/cfsfile/__key/communityserver-wikis-components-files/00-00-00-05-58/PLAXIS2DCE_2D00_V20.04_2D00_1_2D00_Tutorial.pdf

Cao, J., Du, J., Zhang, H., He, H., Bao, C., and Liu, Y. (2024). Mechanical properties of multi-bolted Glulam connection with slotted-in steel plates. *Constr. Build. Mater.* 433, 136608. doi:10.1016/j.conbuildmat.2024.136608

Damians, I., Bathurst, R., Lloret, A., and Josa, A. (2016). Vertical facing panel-joint gap analysis for steel-reinforced soil walls. *Int. J. Geomech.* 16 (4), 040151031–40151114. doi:10.1061/(ASCE)GM.1943-5622.0000632

Du, C., Xu, Z., Yi, F., Gao, J., and Shi, K. (2023). Bearing capacity mechanism of soilbagged graphite tailings. *Bull. Eng. Geol. Environ.* 83 (1), 24. doi:10.1007/s10064-023-03531-7

Dulal, T., and Kumar Yadav, S. (2021). Study of the effect of geogrid on the stability of embankment. *10th IOE Grad. Conf.* 10, 2350–8914.

Federal Highway Administration (2019). Development of a comprehensive bridge management system. Available at: https://www.fhwa.dot.gov/publications/research/infrastructure/structures/bridge/19024/19024.pdf.

Huang, H., Xue, C., Zhang, W., and Guo, M. (2022). Torsion design of CFRP-CFST columns using a data-driven optimization approach. *Eng. Struct.* 251, 113479. doi:10.1016/j.engstruct.2021.113479

Huang, H., Yao, Y., Zhang, W., and Zhou, L. (2023). A push-out test on partially encased composite column with different positions of shear studs. *Eng. Struct.* 289, 116343. doi:10.1016/j.engstruct.2023.116343

Kost, A., Filz, G., Cousins, T., and Carey Brown, M. (2014). Full-scale investigation of differential settlements beneath a geosynthetic-reinforced soil bridge abutment. *Transp. Res. Rec.* 2462 (1), 28–36. doi:10.3141/2462-04

Lu, D., Ma, C., Du, X., Jin, L., and Gong, Q. (2017). Development of a new nonlinear unified strength theory for geomaterials based on the characteristic stress concept. *Int. J. Geomechanics* 17 (2). doi:10.1061/(ASCE)GM.1943-5622.0000729

Mohamed, K., Abouzakhm, M., and Elias, M. (2012). Applications and performance of geosynthetic-reinforced soil abutments on soft subsurface soil conditions. *Transp. Res. Rec.* 1, 74–81. doi:10.3141/2212-08

Mulabdic, M., Minažek, K., and Kaluđer, J. (2018). "Geogrids - what is important," in *Fifth international conference on road and rail infrastructure*, 215–221. doi:10.5592/CO/CETRA.2018.934

Murtaza Rasool, A., Niazi, F., Ahmed, T., and Aziz, M. (2023). A parametric investigation on effect of supporting arrangements on earth retention system. *Geomech. Eng.* 33, 507–518. doi:10.12989/gae.2023.33.5.507

National concrete masonary association (2019). GRS IBS: solutions to bridge construction challenges. Available at: https://ncma.org/updates/news/grs-ibs-solutions-to-bridge-constructionchallenges/.

Rashid, S. I., and Yousaf Shah, M. (2021). State-of-the-Art review on the role of geocells in soil reinforcement. *Geotech. Geol. Eng.* 39, 1727–1741. doi:10.1007/s10706-020-01629-3

Saghebfar, M., Abu-Farsakh, M., Ardah, A., Chen, Q., and Fernandez, B. (2017). Performance monitoring of geosynthetic reinforced soil integrated bridge system (GRS-IBS) in Louisiana. *Geotext. Geomembr.* 45 (2), 34–47. doi:10.1016/j.geotexmem.2016.11.004

Saquib Wani, K., and Mir, B. (2020). Stabilization of weak dredged soils by employing waste boulder crusher dust: a laboratory study. *Geotech. Geol. Eng.* 38 (2), 6827–6842. doi:10.1007/s10706-020-01472-6

Soo, W. M., and Patinga, L. C. (2021). Numerical analyses on the behavior of geosynthetic-reinforced soil: integral bridge and integrated bridge system. *Appl. Sci.* 11 (17), 2–23. doi:10.3390/app11178144

Tahasildar, J., Erzin, Y., and Hanumantha Rao, B. (2018). Development of relationships between swelling and suction properties of expansive soils. *Int.J. Geotech. Eng.* 12 (1), 53–65. doi:10.1080/19386362.2016.1250040

Talebi, M., and Meehan, C. (2015). Numerical simulation of a geosynthetic reinforced soil integrated bridge system during construction and operation using parametric studies. *IFCEE* 2012, 1493–1502. doi:10.1061/9780784479087.135

Talebi, M., Meehan, C., Cacciola, D., and Becker, M. (2014). *Design and construction of a geosynthetic reinforced soil integrated bridge system*. Atlanta Georgia, United States: Geo-congress, 4176–4190. doi:10.1061/9780784413272.406

U.S. Department of transportation (2020). Federal highway administration, GRS IBS bridges. Available at: https://highways.dot.gov/federal-lands/programs-tribal/bridge/grs-ibs-bridges.

Wu, J., and Pham, T. (2013). Load-carrying capacity and required reinforcement strength of closely spaced soil-geosynthetic composites. *J. Geotech. Geoenvironmental Eng- ASCE* 139 (9), 1468–1476. doi:10.1061/(ASCE)GT.1943-5606.0000885

Xie, Y., and Leshchinsky, B. (2015). MSE walls as bridge abutments: optimal reinforcement density. *Geotext. Geomembr.* 43 (2), 128–138. doi:10.1016/j.geotexmem.2015.01.002

Xu, C., Luo, M., Shen, P., Han, J., and Ren, F. (2020). Seismic performance of a whole geosynthetic reinforced soil – integrated bridge system (GRS-IBS) in shaking table test. *Geotext. Geomembr.* 48, 315–330. doi:10.1016/j.geotexmem.2019.12.004

Zheng, Y., and Fox, P. (2017). Numerical investigation of the geosynthetic reinforced soil–integrated bridge system under static loading. *J. Geotech. Geoenvironmental Eng.-ASCE* 143 (6), 040170081–40170114. doi:10.1061/(ASCE)GT.1943-5606.0001665

Zheng, Y., Fox, P., and McCartney, J. (2018). Numerical study on maximum reinforcement tensile forces in geosynthetic reinforced soil bridge abutments. *Geotext. Geomembr.* 46 (5), 634–645. doi:10.1016/j.geotexmem.2018.04.007